communications biology

A Nature Portfolio journal

Article

https://doi.org/10.1038/s42003-025-08049-0

Influence of the phytoplankton community structure on the southern elephant seals' foraging activity within the Southern Ocean

Ziad Sari El Dine [1,2] ✉, Christophe Guinet [1], Baptiste Picard [1], Melilotus Thyssen [3], Lucile Duforêt-Gaurier[2] & Roy El Hourany [2]

The intricate relationship between trophic levels in marine ecosystems remains largely unexplored, particularly in the Southern Ocean. To investigate the complex composition of water constituents, notably the phytoplankton community, we used machine learning techniques to classify six bio-optical classes from a comprehensive ocean-color data time-series. In situ data from the Southern Ocean further characterized these classes by predominant phytoplankton types. Bio-logging data from southern elephant seals revealed that 60% of prey-catch attempts were concentrated within the diatom-dominated class, despite its lower regional frequency. Seals exhibited enhanced foraging activity and prolonged residency periods, up to 42 consecutive days, in diatom-rich waters compared to 5-10 days in other classes. These findings suggest a preference among southern elephant seals for diatom-rich waters, indicating a selective foraging activity influenced by the phytoplankton community's structural composition rather than total biomass alone. This preference underscores the intricate interplay between marine top predators and ecosystem dynamics, hinting at mechanisms through which phytoplankton structure shapes seal activity.

The Southern Ocean accounts for up to half of the annual oceanic uptake of anthropogenic CO_2 and supplies nutrients that sustain the global ocean's biological productivity[1]. Recent observations indicated that large-scale changes are occurring in the Southern Ocean, such as circumpolar warming that exceeds the global average, freshening due to ice melt, and changes in the hydrological cycle[1]. Indeed, climate change models predict that ocean warming would be more pronounced at higher latitude regions, causing large-scale changes in marine ecosystems[2,3].

Climate change is notably influencing the phytoplankton community structure[4], which is the base of the global oceanic food web and contributes to more than half of global primary production[5]. Thus, any climate-induced change in the structure of the Southern Ocean phytoplankton communities could ripple through the food chain, generating a trophic cascade and ultimately affecting top predators such as the southern elephant seal (*Mirounga leonina*)[6]. The behavior and performance of these predators give insight into the spatial and temporal variation of the lower trophic levels, shedding light on ecosystem-level changes[7]. Indeed, the southern elephant seal (SES) proved to be an exceptional candidate for bio-logging, providing crucial information about their physical, biogeochemical, and ecological environment, even in the most remote regions of the Southern Ocean where human monitoring is limited[3,8–11]. Recent observations indicated a decrease in the blood $\delta^{13}C$ values of SES pups over a decade (2004–2018) within the Indian sector of the Southern Ocean, suggesting ecological changes in the region[3]. SES pups receive their nutrients solely from their mothers' milk which reflects the adult female SES foraging activity. With no significant changes in the at-sea distribution or apparent shifts in the habitual foraging grounds of adult female SES, this decrease was hypothesized to be linked to alterations in the phytoplankton community structure[3]. For instance, the decrease could be attributed to the replacement of ^{13}C-rich phytoplankton, such as diatoms, with ^{13}C-depleted nano- and picophytoplankton[12]. Taken together, these findings imply a potential association between the foraging activity of SES and the dynamics of the phytoplankton community in the Southern Ocean. Therefore, disentangling the relationship between the phytoplankton community structure and the SES in the present era is crucial to understanding potential cascading responses to climate-induced changes in the Southern Ocean. In our analysis, we utilized "prey-catch attempt" data as an indication of SES foraging success and prey availability. This is due to a recent publication by Chevallay et al.[13], where the foraging activity of the SES

[1]Centre d'Etudes Biologiques de Chize, CEBC-CNRS UPR 1934, F 79360 Villiers en Bois, France. [2]Laboratoire d'Oceanologie et de Géosciences, Univ. Littoral Côte d'Opale, Univ. Lille, CNRS, IRD, UMR 8187, F 62930 Wimereux, France. [3]Aix Marseille Université, Université de Toulon, Centre National de la Recherche Scientifique, Institut de Recherche et de Développement, Mediterranean Institute of Oceanology, F 13100 Marseille, France.
✉e-mail: ziad.sari-el-dine@cebc.cnrs.fr

was studied relying on a miniature echo-sounder (i.e., micro-sonar) allowing to assess acoustic prey size and prey response behavior to approaching SES. This study suggested that the probability of success for each SES prey-catch attempt is very high and that "prey-catch attempts" could act as an indicator of successful prey captures. It also showed that the mean prey size ranged from 5.0 to 9.0 cm (first and third quantiles, Q1–Q3) with a mean prey size of 7.2 ± 3.1 cm. Therefore, we could assume that an increase in the rate of prey-catch attempts signifies an increase in foraging success.

A recent study analyzed a time series of Aqua-MODIS remote sensing reflectance (R_{rs}) products to address climate-induced changes in the water optical signature[14,15]. The R_{rs} is the ratio between the water-leaving radiance and the downwelling irradiance, acting as an indicator of water constituents (i.e., phytoplankton cells in open water) interacting with light. This study showed that the optical information is changing at the surface of the oceans, potentially hinting at changes in the phytoplankton communities. Given the fact that the Southern Ocean is one of the most under-sampled regions of the global ocean due to the vastness and remoteness of the area, ocean-color remote sensing is an efficient tool to monitor the phytoplankton assemblage of this ecosystem[9,16]. Early methods utilizing ocean color data were centered around estimating chlorophyll-a (Chl-a) concentration as it is commonly used as a proxy for the phytoplankton biomass in surface waters[17]. Recently, research has focused on estimating characteristic properties of phytoplankton communities, such as the dominant phytoplankton functional type (PFT)[18], the size structure[19], or the relative abundance of several PFTs relying on specific optical signatures[20–22]. Indeed, the optical signature perceived by ocean-color satellites holds valuable information on the community composition of phytoplankton and has been used to address questions related to long-term ecosystemic changes in the upper ocean layer[15].

Due to the lack of a dedicated regional algorithm that investigates the phytoplankton community structure from satellite data in the Southern Ocean, we chose to investigate the SES environment (Fig. 1) using the satellite-derived optical signatures as a proxy of phytoplankton community changes. In this work, a long time-series (2003–2021) of ocean color satellite images, centered around the Kerguelen Islands (Fig. 1), was used to define different bio-optical "water-type" classes. The choice of the studied region was to account for all areas that are accessible to the Kerguelen elephant seals during foraging trips. To identify the classes, we employed machine learning techniques, classifying the data through a self-organizing map and a hierarchal ascending classification. The parameters defining the classes, Chlorophyll-a (Chl-a), sea surface temperature (SST), and the remote sensing reflectance at different wavelengths ($R_{rs}(\lambda)$), highlight different aspects of the phytoplankton communities presented in this region. The Chl-a is a proxy of the total phytoplankton biomass, the SST describes the physical conditions of the region as a proxy of time, seasons, heat transport, and currents, and the $R_{rs}(\lambda)$ could detect different phytoplankton groups through specific spectral changes in response to their pigment content and their morphology[15,20]. A daily time series of maps representing the temporal and spatial distribution of the water-type classes was generated and used to visualize monthly climatologies. Utilizing the Southern Ocean in-situ high-performance liquid chromatography (HPLC) and automated flow cytometry (MAP-IO) data, we then associated each class with a certain phytoplankton community structure. Finally, we studied the relationship between female SES residency time and prey-catch rate according to the phytoplankton assemblages encountered represented by the water-type classes. The objective was to demonstrate if the seals are expressing a selective preference amongst the different classes, and consequently amongst different phytoplankton community structures, during foraging trips, and if there is a causal relationship between the presence of a specific class and the overall foraging activity of the seals. This would signify if the seals' foraging activity is influenced by the phytoplankton community structure, or solely by the phytoplankton biomass, regardless of the type of phytoplankton present.

Results and discussion

Regional characterization of bio-optical water types in terms of phytoplankton community structure

After processing and analyzing the satellite data, we identified 6 water-type classes that adequately represent the major patterns in this region in terms of Chl-a, SST, and the $R_{rs}(\lambda)$. Boxplots illustrating the ranges of Chl-a concentrations and SST per class, along with a line graph showing the mean normalized R_{rs} spectral shapes across different wavelengths, were constructed to characterize the classes using the classification method (Fig. 2a). Class 2 exhibits the lowest Chl-a concentrations (approximately 0.05 mg m^{-3}) and the highest SST range, which is almost always above 20 °C. Classes 1, 3, 4, and 6 display moderate to high Chl-a concentrations (0.1–0.25 mg m^{-3}), whereas class 5 distinctly shows the highest Chl-a values, reaching up to 0.4 mg m^{-3}. These results indicate that class 5 represents the most productive waters, while class 2 corresponds to oligotrophic waters confined to the lowest latitudes of the studied region. Furthermore, classes 2 and 5 exhibit contrasting characteristics in terms of the R_{rs} spectrum, reflecting ultra-oligotrophic conditions for class 2 and eutrophic conditions for class 5.

To characterize the water-type classes in terms of phytoplankton community structure, we integrated multi-source in-situ datasets (Supplementary Note 1), including HPLC pigment analyses and MAP-IO flow cytometry data (Table 1). The HPLC dataset provided insights into dominant pigments, reflecting the composition of phytoplankton communities. We should note that pigments overlap within phytoplankton taxonomic groups (for example fucoxanthin being present in both diatoms and haptophytes), and therefore complementary sources such as cytometry data are

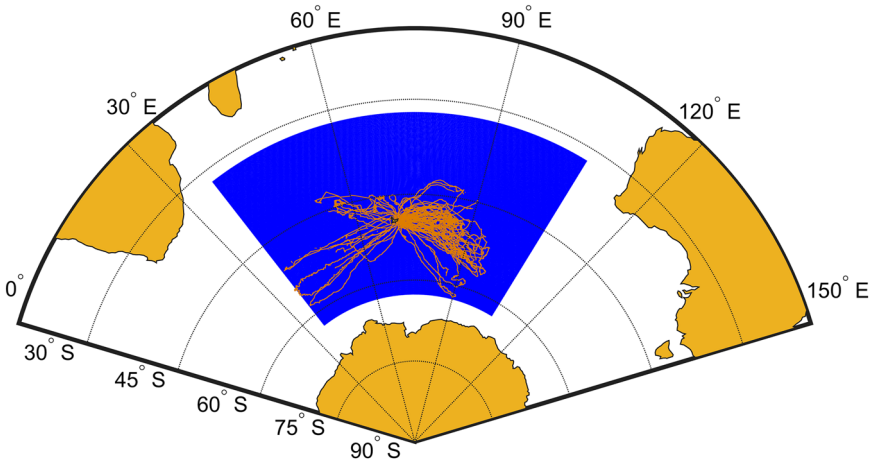

Fig. 1 | The studied area of interest with Southern elephant seal tracks. Map showing the region of interest in the Southern Ocean where the satellite images were retrieved (blue) along with the elephant seal tracks compiled between 2010 and 2020 (orange).

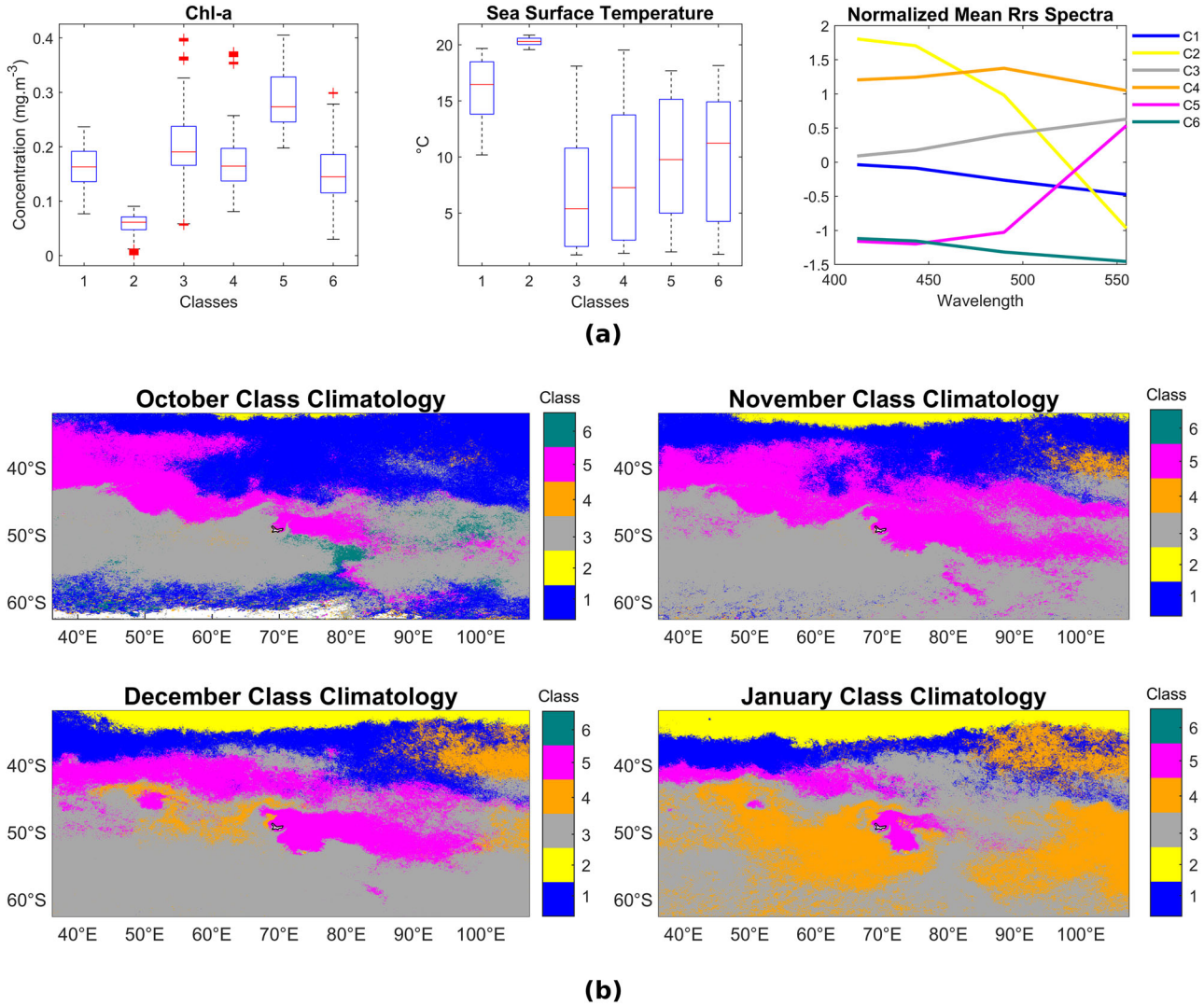

Fig. 2 | Characterization of the water-type classes in terms of the satellite data in addition to a monthly class climatology over the area of interest. a Boxplots (red line = median; upper and lower box limits = 75th and 25th percentiles; dotted line limits: upper and lower adjacents; red crosses = Outliers) showing the Chl-a concentration and the SST ranges per class, in addition to the mean normalized R_{rs} spectral shapes per class, determined after the classification of the satellite data via a self-organizing map and a hierarchal ascending classification. **b** Climatology of the classes over the studied region for the months where elephant seal prey–catch attempt (PrCA) data is available, between 2003 and 2021.

needed. For this, the MAP-IO flow cytometry dataset complementarily validates these classifications through measurements of cell fluorescence and size-class abundances. Together, these datasets enabled a robust characterization of the water-type classes.

From the HPLC datasets, class 2 is distinguished by pigments such as zeaxanthin and divinyl-Chl-a (Table 1), consistent with prokaryote-dominated phytoplankton communities. The MAP-IO dataset further confirms the presence of prokaryotes, as it shows notable contributions from the OraPicoProk group, defined as photosynthetic cyanobacteria, typically identified as *Synechococcus spp.* [23]. Consequently, class 2 is labeled as being dominated by prokaryotes. Classes 1 and 4 are characterized by the pigments zeaxanthin and 19′-Hexfucoxanthin, indicative of contributions from prokaryotes (picophytoplankton) and haptophytes (nanophytoplankton), respectively. For class 1, the MAP-IO dataset indicates the presence of picophytoplankton, with high relative contributions from the OraPicoProk group and the polyphyletic group RedPico, defined as cells with a diameter <3 µm. Classes 1 and 4 describe a co-dominance, with dominant contributions from prokaryotes and haptophytes. Classes 3 and 5 are characterized by both 19′-Hexfucoxanthin and fucoxanthin pigments, the latter being indicative of the presence of diatoms. According to the MAP-IO dataset, class 3 is described by contributions from the RedPico and RedNano groups. The RedNano group, a polyphyletic group that includes phytoplankton cells ranging in size from approximately 3 to 20 μm, is consistent with the presence of haptophytes and diatoms. Therefore, class 3 is identified as a class with co-dominant contributions from haptophytes and diatoms. Class 5 is characterized by the RedNano and RedMicro groups, with the latter being consistent with large diatom cells or diatom chains >20 µm. As class 5 exhibits the highest fucoxanthin concentrations and the greatest fluorescence contributions from the RedNano and RedMicro size classes, it is identified as diatom-dominated. Finally, class 6 is characterized by 19′-Hexfucoxanthin, with contributions from the RedPico and RedNano size classes, further indicating the presence of haptophyte-dominated communities.

To further compare our findings, we analyzed the correspondence between PHYSAT spectral signature classes and each water-type class determined by our approach (see SI, Fig. S1). The distribution of PHYSAT classes across different water-type classes revealed distinct community structures within each class. Since PHYSAT identifies water-leaving radiance anomalies while minimizing the influence of biomass-based signals,

Table 1 | Water-type classes characterization

Class	Chl-a (Avg. mg m^{-3}) (±std) Source: Globcolour	SST (Avg. °C) (±std) Source: MODIS Aqua	Dominant PFT Labels	Dominant Pigment Source: HPLC	Cytometry group's highest relative contribution Source: MAP-IO Flow Cytometry	PHYSAT Dominant PFT Source: PHYSAT Database
1	0.16 (±0.03)	15.98 (±2.8)	Prokaryotes/Haptophytes	Zeaxanthin/19'Hexfucoxanthin	RedPico/OraPicoProk	Prochlorococcus/Cyanobacteria
2	0.05 (±0.01)	20.27 (±0.4)	Prokaryotes	Zeaxanthin/Divynil-Chl-a	OraPicoProk	Prochlorococcus/Cyanobacteria
3	0.20 (±0.06)	6.91 (±5.3)	Haptophytes/Diatoms	Fucoxanthin/19'Hexfucoxanthin	RedPico/RedNano	Phaeocystis-like
4	0.17 (±0.05)	8.67 (±6.3)	Haptophytes/Prokaryotes	Zeaxanthin/19'Hexfucoxanthin	–	Phaeocystis-like
5	0.29 (±0.05)	9.76 (±5.4)	Diatoms	Fucoxanthin/19'Hexfucoxanthin	RedNano/RedMicro	Diatoms
6	0.15 (±0.06)	9.65 (±5.8)	Haptophytes	19'Hexfucoxanthin	RedPico/RedNano	Phaeocystis-like

Characterization of the water-type classes in terms of phytoplankton groups and other descriptors through the use of multi-source in-situ and remote sensing data.

this result indicates that the classes are optically distinct and represent unique phytoplankton structures, independent of Chl-a concentration. Specifically, class 5 represents a unique phytoplankton community structure dominated by diatoms. In contrast, classes 3, 4, and 6 are characterized by heterogeneous communities dominated by haptophytes (initially labeled as Phaeocystis-like phytoplankton by PHYSAT), while classes 1 and 2 correspond to prokaryote-dominated phytoplankton communities. This multi-source data analysis underscores the significant distinctions among classes in terms of phytoplankton community structures.

To highlight the major patterns in the spatio-temporal variability of these bio-optical water-type classes, a monthly climatology of the classes was constructed (2003–2021, dominant class per pixel) over the studied region during the months where SES observations are available, i.e., October through January (Fig. 2b). Water-type class 3 was the most prevalent and consistent over the whole region. It is clear that the water-type classes are influenced by currents and fronts. For instance, class 2 waters are limited to the subtropical zone and exhibit high-temperature gradients, evidencing the presence of a subtropical front, which is a density-driven front. Class 5 waters appear to be related to the polar frontal zone, and its spread is influenced by the Antarctic circumpolar current. In addition to that, this class, rich in Chl-a and dominated by diatoms, is consistently present in the eastern side of Kerguelen. The Kerguelen Plateau supports one of the most productive regions in the Antarctic Circumpolar Circulation and enriches waters thousands of kilometers downstream via lateral advection[24], indicating a potential link between class 5 and biological advection resulting from currents and fronts. Seasonally persistent phytoplankton blooms have been shown to occur over the northern plateau, southern plateau, and eastern flank of the southern plateau of Kerguelen[25]. These persistent blooms are sustained by a consistent supply of dissolved iron[26]. Therefore, the consistent appearance of class 5, characterized by the highest Chl-a (an indicator of total phytoplankton biomass) and dominated by diatoms (rapidly increase in the presence of nutrients), agrees with the available literature[24]. In fact, in a recent study[27], an extensive 26-year-long compilation of phytoplankton pigments in the Southern Ocean was studied, and it was shown that diatoms and haptophytes dominate the region around Kerguelen, specifically extending eastwards. Curiously, from Fig. 2b, we can see that the occurrence of class 5 is diminishing and being replaced by class 4 when approaching December-January. This could be explained by the competition present in this region between diatoms and haptophytes, where there is a seasonal cycle of diatom-haptophyte dominance[28].

Linking Southern Elephant Seal activity to bio-optical water-type classes; influence of the phytoplankton community structure

After describing each water-type class in terms of phytoplankton community structure, we introduced the SES data and looked at the relationship between the water-type classes and the SES foraging data. The SES data consisted of unique seal identifiers, the latitude, longitude, and time of observation, and the frequency of prey capture attempts (PrCA), a proxy of the seals' foraging activity. Each SES datapoint was associated, according to the location and date on a 4 km resolution gridded image, with the corresponding water-type class. The PrCA was also normalized based on the variance for comparative purposes among seals and was denoted as NormPrCA.

First, foraging trips of two tagged SES were used for this analysis. Each track targeted a different regime, with the first to the West of Kerguelen, a less productive region, and the second to the East in a more productive region (bloom/post-bloom region) (Fig. 3). Regardless of the direction or foraging region, it can be seen that most bio-logging observations are originating from class 5, the most productive class dominated by diatoms. This signifies that regardless of the foraging regime or location, SES encounter better foraging conditions within productive diatom-dominated waters and, thus, remain in class 5 for the majority of their foraging trip. It is also clear that the NormPrCA peaks are observed when the SES are present in class 5 waters.

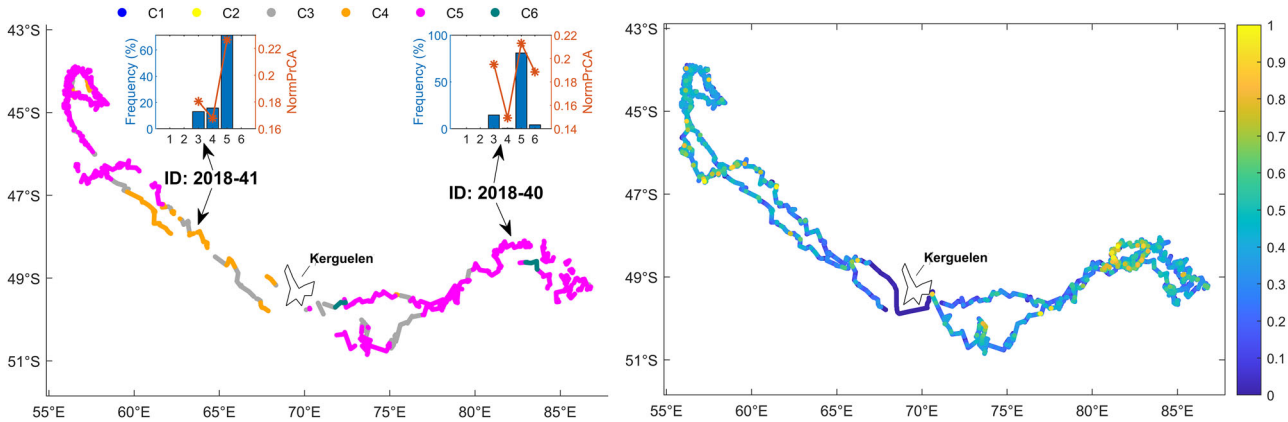

Fig. 3 | The tracks of two individual seals during their foraging trips as a function of water-type classes and normalized prey-catch attempts. Two individual SES tracks with different foraging regimes during 2018, where "2018–2041" forages to the west of Kerguelen between 23 October and the second of January, while "2018–2040" forages to the east between 22 October and the first of January. The plot on the right highlights the value of the NormPrCA at each bio-logging observation. The plot on the left highlights the water-type class at each SES bio-logging observation collected during the foraging trips. The mismatch between observations' density in both plots is mainly due to unavailable satellite matchups when cloud conditions or poor-quality pixels occur. Bar graphs for each SES showing the frequency of each water-type class encountered during the trip (blue bars), as well as the mean NormPrCA plotted per class (orange star and line), are included.

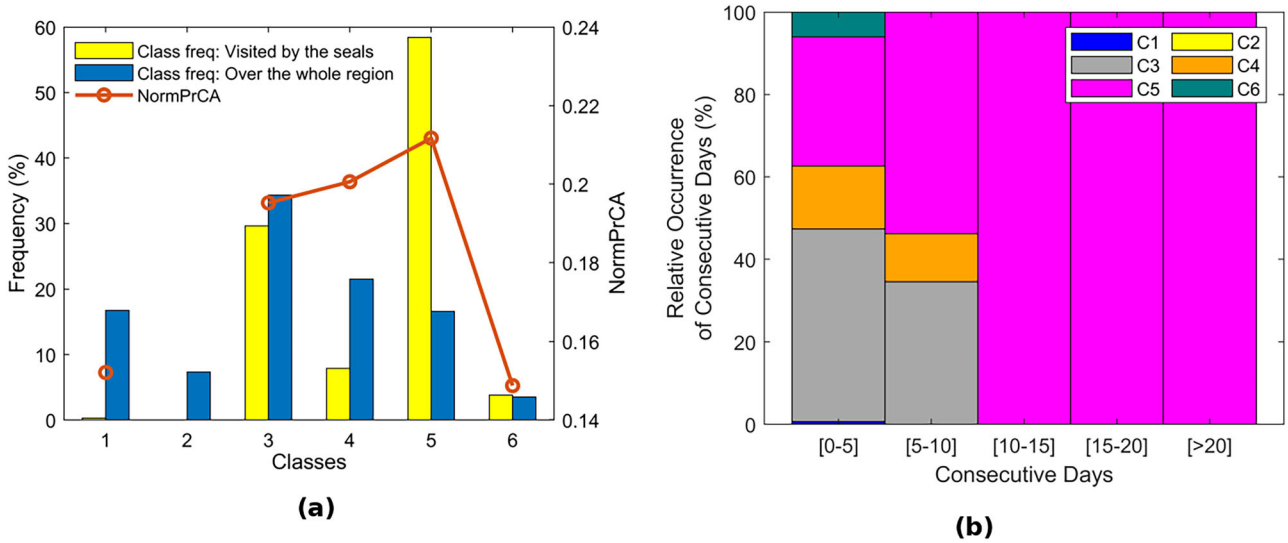

Fig. 4 | Linking the water-type classes with the Southern elephant seal foraging activity. a The frequency of class occurrence in the whole region (blue bars) and in the regions visited by the seals (yellow bars) in addition to the average normalized PrCA per class. **b** The relative occurrence of consecutive days per class, based on 79 SES.

To answer whether these findings can be generalized as SES-preferred conditions, the following analysis was performed on the entire dataset of all SES individuals ($N = 79$), allowing a more generalized view. The frequency of the classes over the whole region was compared with the frequency of the classes where the SES were recorded by the bio-loggers, whether a prey-catch attempt occurred or not, over the same time frame (Fig. 4a). Class 3 is the most frequently occurring water-type class over the whole region with an overall frequency of around 34%, followed by class 4 at 20%, class 1 at 18%, and class 5 at 16%. However, when looking at the frequency of water-type classes visited by the elephant seals, the frequency of class 5 is remarkably greater than all other classes at around 60%, followed by class 3, the most prevalent class regionally, at 30%. In addition to that, it can be seen that the SES demonstrate the highest foraging activity within the waters of class 5.

To better display the significance of the frequency of each water-type class visited by the seals, we calculated the time length of the stay of the seals within the waters of a single class in terms of consecutive days (Fig. 4b). For a time length between 1 and 5 consecutive days, the SES remain and record observations mostly in classes 3 and 5 with a relative frequency of around 40% and 30%, respectively. However, as the time length of the stay in a water-type class increases, it can be seen that the SES remains mostly in class 5. For 10 consecutive days and greater, the SES is solely recorded within class 5, reaching a maximum of 42 consecutive days within this water-type class. The high frequency for class 3 in the 1–5 consecutive day range could be explained by the fact that it is the most prevalent class regionally and, during the foraging trip, the SES could come across this class, but they would not reside in it for a long period of time. During their foraging trips, SES typically follow three distinct phases: (1) an outbound transit phase, where they travel away from the island in search of an optimal foraging ground, (2) a feeding phase, during which they remain in a specific area for an extended period, and (3) a return transit phase, where they travel back to the island[29]. The optimal feeding ground is hypothesized to be influenced by prey aggregations, specific prey types, or oceanic features such as inter-frontal zones and physical ocean structures[29]. Figure 4 indicates that the highest number of consecutive foraging days occurs exclusively in class 5 waters, suggesting that this class offers the most favorable conditions for SES, where their foraging activity is maximized.

Some early studies have shown that no clear relationship between the foraging activity of predators and phytoplankton existed[30,31]. However, Guinet et al.[32] demonstrated that the diving activity of marine predators could be related to the Chl-a concentration. It has been later shown that the deep-diving southern elephant seals recorded more prey-encounter events and performed significantly shallower dives below high-density patches of phytoplankton[33]. In our study, the highest PrCA levels were associated with class 5, which is characterized by the highest Chl-a concentrations (Fig. 2a, Table 1).

However, this work clearly shows that it is not only the influence of Chl-a concentration that dictates the favorable foraging conditions of the SES, but also the phytoplankton community structure present. A Spearman rank correlation was performed between the NormPrCA and the Chl-a and water-type classes (Suppl. Fig. S2). The strongest positive correlation was found between NormPrCA and class 5 ($R_{sp} = 0.19$) and was double that of Chl-a ($R_{sp} = 0.09$). This signified that the foraging activity of the SES does not depend on the Chl-a concentration, a proxy of phytoplankton biomass, but suggests a direct link with the presence of a diatom-dominated community structure.

Finally, to look at any link between prey size and water-type classes, we used new data on SES acoustic prey size determined from micro-sonar devices deployed on 9 SES between 2018 and 2020[13] (Supplementary Note 2). The water-type class corresponding to each observation was retrieved, and the prey size distribution targeted within each class, along with the average number of prey encountered per day within each class, were analyzed (Suppl. Fig. S3). It was shown that there were no significant differences in the size of the prey targeted within all classes; however, a significantly larger amount of prey was targeted within class 5 compared to the other classes, aligning with the PrCA conclusions.

Unless the nutritional value of SES prey, having comparable sizes, varies according to the different water-type classes, our results strongly support that SES might exhibit a preference in the size distribution of targeted prey and that these estimates of prey size, as sampled by SES, might represent a narrow proportion within the size spectrum of mid-trophic levels in the SO. Future studies should aim at better characterizing how the biomass and composition of the Mid-Trophic levels may vary according to the water-type classes, but this is beyond the scope of this study.

Three non-exclusive hypotheses could explain how a preferred water-type class, characterized by high Chl-a and a diatom-dominated community structure, could influence the foraging activity of the SES. (1) An increase in phytoplankton biomass increases the availability of prey to the SES; however, if the biomass of phytoplankton is the major driver of the foraging activity of SES, there should have been a stronger correlation between PrCA and the Chl-a concentration. (2) Increases in the phytoplankton abundance form dense patches on the surface of the ocean. Phytoplankton cells, according to their pigment content, morphology, and tendency to aggregate into chains, impact light attenuation differently[34–36]. The attenuation properties of cells result in a shading effect underneath the surface and draw myctophids, the main prey of SES, to shallower depths, thus facilitating vertical access to prey for the seals during the day. (3) And finally, in the presence of diatoms, a food web more favorable to the elephant seals is formed and better foraging conditions are observed. A possible mechanism is that diatom-rich waters could enhance prey availability indirectly by attracting zooplankton species that serve as primary prey for myctophids and squid, key components of the SES diet. This would create an alternative pathway linking phytoplankton community structure to SES foraging activity, potentially complementing or even competing with the lightscape theory. Further investigation into prey distribution and behavior in relation to phytoplankton composition would be necessary to disentangle these effects. This final hypothesis could explain the selective preference the seals are showing for class 5 as their main foraging grounds.

Conclusion

In this work, a machine learning approach was used to classify the different water types observed in a large region in the Southern Ocean in terms of several bio-optical variables. The classes were then characterized using in-situ data from that same region to associate a phytoplankton community structure to each class. It was shown that the female SES display a selective preference to forage for prolonged periods of time within chlorophyll-rich diatom-dominated waters. It was also shown that these SES demonstrate the highest foraging activity within these waters. It seems that the presence of diatoms positively influences the activity of the SES. Future studies should further explore the dynamics of this relationship. The activity of the SES should be compared during daytime and nighttime to support or refute the hypothesis of the shading effect. Bio-logging studies should be performed utilizing micro-sonar and bioluminescence sensors, among others, and information about the mid-trophic levels should be examined[37,38], clarifying the relationship between the lowest (phytoplankton) and highest (SES) trophic levels[39]. It would also be interesting to investigate if any relationship exists between the bioluminescence present, measured through a bio-logging device, and the different phytoplankton functional types. Finally, it would be worth investing time in conducting a comprehensive trends analysis for the water-type classes/phytoplankton community structure in the Southern Ocean, which can allow us to track any long-term change in the overall phytoplankton community structure in that region, and how it may influence the activity of the SES.

Methods

Bio-optical water-type classification

The self-organizing map (SOM), introduced by Kohonen[40], is an unsupervised classification method. It is based on the k-means algorithm, with the addition of a topological ordering. Thus, the SOM is used to reduce the dimensionality and enhance the interpretability of data, where closely related data would be grouped into one neuron, and neighboring neurons would consist of more similar data, which are relatively close in the actual data space (Euclidean Norm).

A long time-series of 8-day averaged satellite images (level 3 mapped —4 km spatial resolution), between 2003 and 2021, was utilized to train a self-organizing map (hereafter $SOM_{Regional}$, Suppl. Fig. S3). These images were centered over a large region around Kerguelen, between 36.2°E and 107.2°E, and between 31.9°S and 62.6°S (Fig. 1), and included the Chl-a, SST, and the $R_{rs}(\lambda)$ products (at $\lambda = 412$, 443, 490, and 555 nm). The Chl-a and the R_{rs} data were retrieved from the GlobColour project (http://www.globcolour.info) and consisted of merged data from multiple satellite sensors. The selected Chl-a product was the 'CHL1', which corresponds to the Chl-a estimation using an algorithm adapted for case 1 waters. These waters represent the open sea where phytoplankton are the main contributors to ocean color. After validating with in-situ HPLC Chl-a data from the Southern Ocean, this satellite Chl-a product was shown to be up to 70% correlated with in-situ Chl-a, having an average RMSE of 0.16 mg m^{-3} ($n = 5451$, $p = 2.5e^{-299}$). The SST product was retrieved from the NASA EarthData Ocean Color project (https://oceancolor.gsfc.nasa.gov/l3/) and provided by the MODIS sensor aboard the Aqua satellite.

Our choice of the range and number of satellite reflectance bands was based on previous works that used similar classification approaches for comparable applications[17,18,20]. In the clear open ocean, the information contained in the remote sensing reflectance (R_{rs}) bands is limited beyond 555nm due to the strong absorption by water, as also mentioned in Xi et al.[41].

The input data, i.e., Chl-a, R_{rs}(412,443,490,555 nm), and SST, were standardized and scaled to homogenize the weights. The $SOM_{Regional}$ was initialized with 198 neurons in order to reconcile the interpretability and representativity of major patterns found in the data. It classifies similar observations in terms of the input products, into a single cluster or neuron of the SOM representing a distinct water type. Additionally, the patterns in neighboring neurons would be more similar than distant ones. The generated $SOM_{Regional}$ was a two-dimensional hexagonal grid of 198 neurons (18 × 11), where each neuron represented a pattern observed in the studied area in terms of the 6 satellite products.

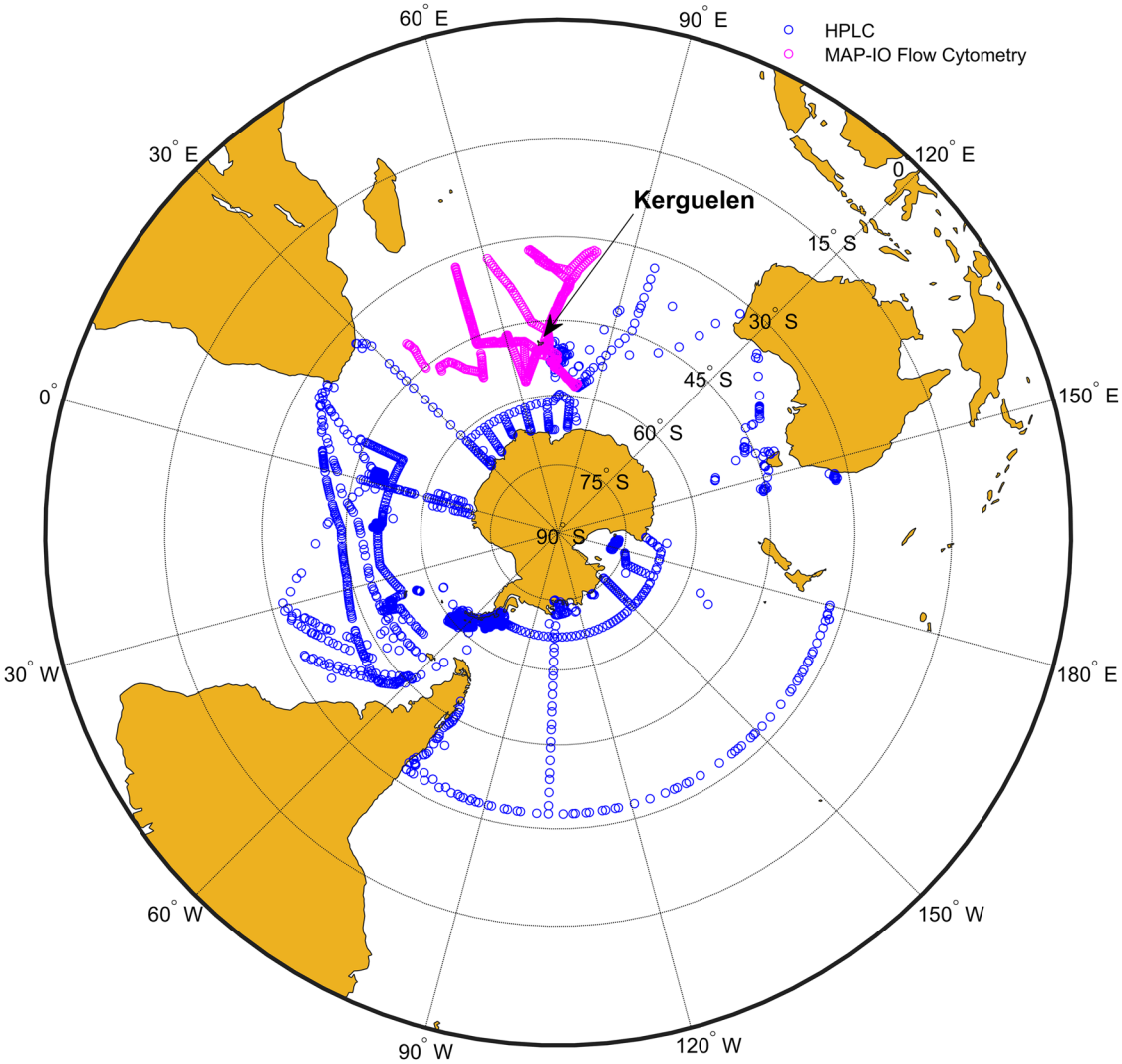

Fig. 5 | The spatial distribution of the in-situ data used. Map showing the distribution of the in situ surface HPLC ($n = 4173$; blue circles) and MAP-IO flow cytometry ($n = 941$; purple circles) observations used. The HPLC data points plotted on the map comprise the publicly available dataset from Soppa et al.[42]. The MAP-IO flow cytometry dataset is also publicly available on SEANOE from Thyssen et al.[45].

A hierarchal ascending classification (HAC) was utilized to group neighboring neurons to further partition the $SOM_{Regional}$ and control the degree of specificity required (Suppl. Fig. S4). The HAC is an automatic classification method that calculates a partition hierarchy, each partition grouping neurons, in an iterative process and based on a metric of similarity (Ward metric, while assuring the topology conservation between neurons within the $SOM_{Regional}$ map). Therefore, the HAC allows the clustering of the $SOM_{Regional}$ neurons representing close or similar patterns in terms of Chl-a, SST, and R_{rs} spectrum, and defines bio-optical classes. The HAC dendrogram (Suppl. Fig. S5) showed that six bio-optical or "water type" classes highlight the major patterns found in the $SOM_{Regional}$, or the studied area. This is determined when a sharp increase in the index of dissimilarity is first observed between the different partitions on the dendrogram.

Characterization of bio-optical water types in terms of phytoplankton community structure

To characterize the water-type classes in terms of phytoplankton community composition, three datasets were introduced in this study: an HPLC pigment dataset, an HPLC-derived Chl-a fraction for phytoplankton groups and finally the MAP-IO flow cytometry dataset.

The first dataset consists of near-surface HPLC secondary phytoplankton pigments compiled in El Hourany et al.[20] and Soppa et al.[42], between 1997 and 2014 (Southern Ocean datapoints: $N = 4173$). Each pigment is used as a marker for major phytoplankton groups[42,43] based on the diagnostic pigment analysis approach (DPA) (see Suppl. Table S1). Supplementary Table S1 shows the pigments included in this dataset with their associated phytoplankton group. The aim of using this dataset is to shed light on the complexity of the phytoplankton community structure.

The second dataset, the MAP-IO flow cytometry dataset, sampled between 2021 and 2023, was introduced[44,45] (Southern Ocean datapoints: $N = 941$). The phytoplankton size classes and groups analyzed are the red (Red-) and the orange (Ora-) Micro, Nano, Pico, Pico Prok, and finally, the HsNano (nanophytoplankton with relatively high sideward light scattering properties) and RedPico_High Fluroscence groups. These groups are expressed in terms of red fluorescence per ml, as the sum of the mean red fluorescence pulse shape per group multiplied by its abundance (MOTFLR/ml), and the abundance of cells per ml. A description of the groups is found in ref. 23.

Among the two databases, only data points corresponding to the Southern Ocean (<32°S) were taken into account (Fig. 5). Satellite matchups for each of the input products used to train the $SOM_{Regional}$ were

retrieved. Each data point of this joint database was associated with a neuron of the $SOM_{Regional}$ based on the satellite matchups and, consequently, associated with a specific water-type class. A quality control threshold based on R_{rs} (as in the work of El Hourany et al.[20]) was used to limit the affectation of abnormal and unseen situations while calculating the distance between a datapoint (characterized by R_{rs} at 4 wavelengths) and the closest neuron to it; this distance is expressed in terms of the number of standard deviations from the referent vector of the closest neuron. Only data points close enough (3 standard deviations) to their associated neuron are accepted. By that, any datapoint outside the region of interest (Fig. 1), and not similar to any situation encountered within the region of interest throughout the time-series in terms of the remote sensing products, was removed by the quality control procedure.

By doing so, each neuron, and therefore each water-type class, is characterized by a distribution of HPLC pigments, Chl-a concentrations for the three phytoplankton groups, and the MAP-IO information on the quantity and group structure of cells.

In addition to that, the satellite-derived PHYSAT data was also introduced. The algorithm behind PHYSAT aims to identify classes characterized by dominant phytoplankton functional (PFT) type based on the detection of spectral anomalies in the normalized water-leaving radiance. These spectral anomalies are linked to specific PFTs by using coincident in-situ measurements of pigment inventories[4]. The PHYSAT database was retrieved from the GlobColour website (http://www.globcolour.info). The data includes a monthly time series of global images representing the dominant PFT per month between 2003 and 2010 at a 9 km spatial resolution. Five PFTs are detected through this algorithm: nanoeukaryotes, cyanobacteria, prochlorococcus, diatoms, and phaeocystis-like. Due to the limited time-frame of the PHYSAT data (reaching 2010 only), the poor spatial resolution, and the need for a Southern Ocean-specific algorithm for water-type description, the PHYSAT product was exclusively used to complementarize the delimited bio-optical class and to highlight qualitatively different phytoplankton communities within each class.

Southern elephant seal and water-type classes analysis

The bio-logging data used were compiled from several previously published literature and data[8,33,46,47]. As stated in the previous studies, the SES were treated in accordance with the IPEV ethical and Polar Environment Committees guidelines. The compiled processed SES data allowed us to study the influence of the phytoplankton communities on the SES foraging activity.

Data highlighting the events of prey capture by adult female SES come from 79 total deployments of bio-loggers between 2010 and 2020. They were collected in the area of the Kerguelen Islands and included: unique seal identifiers, dates and coordinates of measurement, and the number of prey capture attempts (PrCA), which were later normalized based on the prey capture attempts of each individual seal (variance) for comparative purposes (NormPrCA). The PrCA was calculated from head acceleration data recorded by accelerometers deployed on the heads of the SES[8,46]. The entire dataset included 227,293 PrCA observations over 681 total days. The PrCA data were available within a limited time frame for each year, ranging from the end of October to the beginning of February. This is explained by the fact that post-breeding-tagged female elephant seals forage at sea for 65–80 days, departing in late October (after the breeding period) and returning to land, where the bio-logging tags are collected, throughout January to molt[8].

The SES can be equipped with different tags. These latter consisted of a range of satellite tags and data loggers. The SES were usually equipped with GPS loggers in combination with Argos satellite loggers and archival data loggers (SPLASH10), transmitting Argos location data and collecting GPS location data. The SPLASH10 devices also included a time-depth recorder (TDR) which recorded pressure, light, and temperature levels at 1 or 2-s intervals. In addition to that, conductivity-temperature-depth satellite-relay data loggers (CTD-SRDLs) combined with either TDR loggers, or TDR-accelerometer data loggers, sample acceleration as well as pressure. These data loggers were glued on the heads of the female SES using quick-setting epoxy. Further details about the devices and the sampling parameters can be found in Guinet et al.[8].

In this study, we used only the data logged from the TDR-accelerometer. TDRs recorded dive depth and duration, allowing identification of foraging dives, while accelerometers captured high-frequency head movements indicative of prey strikes. PrCA events were detected by analyzing rapid head-jerk movements, which have been validated as indicators of prey capture in marine predators[46,47]. These accelerometer-derived signals were synchronized with TDR dive profiles to ensure they occurred during active foraging. Tags transmit their pooled information upon the surfacing of the SES between dives[8].

Some seals have partial tracks recorded since some bio-loggers would stop recording during the foraging trip. However, in our study, this only influenced the relative occurrence of consecutive days per class result (Fig. 4b) by giving more weight to the lower ranges of consecutive days.

Each PrCA observation was associated with a water-type class through the retrieval of satellite match-ups based on the date and location of each seal observation. For each observation, we identified the closest 10×10-pixel box (each pixel at 4 km resolution) surrounding the coordinates of the observation on the same day. From this data, we estimated two key quantities: (1) the frequency of water-type classes within the 10×10-pixel area (only when 50% of pixels are available within this area), which was used for correlation analysis (Suppl. Fig. S2), and (2) the class of the closest pixel, which was directly assigned to the observation for further analysis. Around 54% of PrCA observations were assigned to satellite matchups.

This dual approach allowed us to account for both the dynamical aspect of the distribution of water-type classes around each observation and the immediate conditions at the precise location and time of the seal's activity.

Statistics and reproducibility

All statistical tests were performed using Matlab, and the results are reported as mean ± standard deviation (std) when appropriate. The significance of the correlation analysis was highlighted with *p*-values (significant if *p*-value less than 0.05). The plots and tables were constructed in a way to show data variability and distribution.

The reproducibility of our results is possible. All the methods are sufficiently described and all underlying data, in addition to supplementary code and Matlab libraries, are publicly available (sources or public repositories mentioned).

For the SES data, they were collected and detailed in the framework of previously published studies[8,33]. For this study, the previously collected and processed SES data were compiled over 10 years. Sample sizes were determined based on available bio-logging devices ready to be deployed and experimental feasibility. Data from 79 adult female SES were used in this study and are available in full with sufficient description on https://doi.org/10.5281/zenodo.11120351.

Reporting summary

Further information on research design is available in the Nature Portfolio Reporting Summary linked to this article.

Data availability

All data used and generated in this study are available at the following public repository[48]: https://doi.org/10.5281/zenodo.11120351. Chl-a, Rrs, and PHYSAT satellite images are found at the http://www.globcolour.infoportal. SST data can be found on the NASA EarthData Ocean Color portal https://oceancolor.gsfc.nasa.gov/l3/, and provided by the MODIS sensor aboard the Aqua satellite. HPLC data from El Hourany et al.[49] can be found on https://doi.org/10.5281/zenodo.10361485and from Soppa et al.[42] at https://doi.org/10.3389/fmars.2017.00203.

Code availability

The code used to train the SOM is available as a MATLAB script in the following public repository[48]: https://doi.org/10.5281/zenodo.11120351.

Received: 25 June 2024; Accepted: 7 April 2025;
Published online: 16 April 2025

References

1. Ducklow, H. W. et al. Marine pelagic ecosystems: the west antarctic peninsula. *Philos. Trans. R. Soc. B* **362**, 67–94 (2007).
2. Constable, A. J. et al. Climate change and southern ocean ecosystems i: how changes in physical habitats directly affect marine biota. *Glob. Change Biol.* **20**, 3004–3025 (2014).
3. Mestre, J. et al. Decadal changes in blood δ^{13}c values, at-sea distribution, and weaning mass of southern elephant seals from Kerguelen islands. *Proc. R. Soc. B* **287**, 20201544 (2020).
4. Alvain, S., Moulin, C., Dandonneau, Y. & Loisel, H. Seasonal distribution and succession of dominant phytoplankton groups in the global ocean: a satellite view. *Global Biogeochem. Cycles* **22**, GB3001 (2008).
5. Behrenfeld, M. J. et al. Biospheric primary production during an ENSO transition. *Science* **291**, 2594–2597 (2001).
6. Drinkwater, K. F. et al. The response of marine ecosystems to climate variability associated with the North Atlantic Oscillation. *Geophys. Monogr. Ser.* **134**, 211–234 (2003).
7. Hindell, M. A. et al. Circumpolar habitat use in the southern elephant seal: implications for foraging success and population trajectories. *Ecosphere* **7**, e01213 (2016).
8. Guinet, C. et al. Southern elephant seal foraging success in relation to temperature and light conditions: insight into prey distribution. *Mar. Ecol. Prog. Ser.* **499**, 285–301 (2014).
9. Deppeler, S. L. & Davidson, A. T. Southern ocean phytoplankton in a changing climate. *Front. Marine Sci.* https://www.frontiersin.org/articles/10.3389/fmars.2017.00040 (2017).
10. Roquet, F. et al. Estimates of the Southern Ocean general circulation improved by animal-borne instruments. *Geophys. Res. Lett.* **40**, 6176–6180 (2013).
11. Treasure, A. M. et al. Marine mammals exploring the oceans pole to pole: a review of the meop consortium. *Oceanography* **30**, 132–138 (2017).
12. Deuser, W. G. Isotopic evidence for diminishing supply of available carbon during diatom bloom in the black sea. *Nature* **225**, 1069–1071 (1970).
13. Chevallay, M., Guinet, C., Goulet, P. & Jeanniard, dD. T. Hunting tactics of southern elephant seals Mirounga leonina and anti-predatory behaviours of their prey. *Mar. Ecol. Prog. Ser.* **736**, 167–179 (2024).
14. Dutkiewicz, S. et al. Ocean colour signature of climate change. *Nat. Commun.* **10**, 578 (2019).
15. Cael, B. B., Bisson, K., Boss, E., Dutkiewicz, S. & Henson, S. Global climate-change trends detected in indicators of ocean ecology. *Nature* **619**, 551–554 (2023).
16. Robinson, C. M. et al. High latitude southern ocean phytoplankton have distinctive bio-optical properties. *Opt. Express* **29**, 21084–21112 (2021).
17. Ben Mustapha, Z., Alvain, S., Jamet, C., Loisel, H. & Dessailly, D. Automatic classification of water-leaving radiance anomalies from global seawifs imagery: application to the detection of phytoplankton groups in open ocean waters. *Remote Sens. Environ.* **146**, 97–112 (2014). Liege Colloquium Special Issue: Remote sensing of ocean colour, temperature and salinity.
18. Alvain, S., Moulin, C., Dandonneau, Y. & Bréon, F. Remote sensing of phytoplankton groups in case 1 waters from global SeaWifs imagery. *Deep Sea Res. Part I* **52**, 1989–2004 (2005).
19. Sathyendranath, S. et al. Phytoplankton functional types from space. *Reports of the International Ocean-Colour Coordinating Group, No. 15* (2014).
20. El Hourany, R. et al. Estimation of secondary phytoplankton pigments from satellite observations using self-organizing maps (soms). *J. Geophys. Res.* **124**, 1357–1378 (2019).
21. Xi, H. et al. Global retrieval of phytoplankton functional types based on empirical orthogonal functions using cmems globcolour merged products and further extension to olci data. *Remote Sens. Environ.* **240**, 111704 (2020).
22. Xi, H. et al. Global chlorophyll a concentrations of phytoplankton functional types with detailed uncertainty assessment using multisensor ocean color and sea surface temperature satellite products. *J. Geophys. Res.* **126**, e2020JC017127 (2021).
23. Thyssen, M. et al. Interoperable vocabulary for marine microbial flow cytometry. *Front. Marine Sci.* **9**, 975877 (2022).
24. Della Penna, A. et al. Mesoscale variability of conditions favoring an iron-induced diatom bloom downstream of the Kerguelen plateau. *J. Geophys. Res.* **123**, 3355–3367 (2018).
25. Schallenberg, C. et al. Sustained upwelling of subsurface iron supplies seasonally persistent phytoplankton blooms around the southern Kerguelen plateau, southern ocean. *J. Geophys. Res.* **123**, 5986–6003 (2018).
26. d'Ovidio, F. et al. The biogeochemical structuring role of horizontal stirring: Lagrangian perspectives on iron delivery downstream of the Kerguelen plateau. *Biogeosciences* **12**, 5567–5581 (2015).
27. Hayward, A., Pinkerton, M. H., Wright, S. W., Gutiérrez-Rodriguez, A. & Law, C. S. Twenty-six years of phytoplankton pigments reveal a circumpolar class divide around the southern ocean. *Commun. Earth Environ.* **5**, 92 (2024).
28. Nissen, C. & Vogt, M. Factors controlling the competition between *Phaeocystis* and diatoms in the southern ocean and implications for carbon export fluxes. *Biogeosciences* **18**, 251–283 (2021).
29. Jonker, F. C. & Bester, M. N. Seasonal movements and foraging areas of adult southern female elephant seals, Mirounga leonina, from Marion island. *Antarct. Sci.* **10**, 21–30 (1998).
30. Bradshaw, C. J., Higgins, J., Michael, K. J., Wotherspoon, S. J. & Hindell, M. A. At-sea distribution of female southern elephant seals relative to variation in ocean surface properties. *ICES J. Mar. Sci.* **61**, 1014–1027 (2004).
31. Jaquet, N. & Whitehead, H. Scale-dependent correlation of sperm whale distribution with environmental features and productivity in the South Pacific. *Mar. Ecol. Prog. Ser.* **135**, 1–9 (1996).
32. Guinet, C. et al. Spatial distribution of foraging in female Antarctic fur seals Arctocephalus Gazella in relation to oceanographic variables: a scale-dependent approach using geographic information systems. *Mar. Ecol. Prog. Ser.* **219**, 251–264 (2001).
33. O'Toole, M., Guinet, C., Lea, M. & Hindell, M. Marine predators and phytoplankton: how elephant seals use the recurrent Kerguelen plume. *Mar. Ecol. Prog. Ser.* **581**, 215–227 (2017).
34. Svensen, Ø., Frette, Ø. & Erga, S. R. Scattering properties of microalgae: the effect of cell size and cell wall. *Appl. Opt.* **46**, 5762–5769 (2007).
35. Boss, E., Slade, W. & Hill, P. Effect of particulate aggregation in aquatic environments on the beam attenuation and its utility as a proxy for particulate mass. *Opt. Express* **17**, 9408–9420 (2009).
36. Moutier, W. et al. Evolution of the scattering properties of phytoplankton cells from flow cytometry measurements. *PLoS ONE* **12**, e0181180 (2017).
37. Goulet, P., Guinet, C., Swift, R., Madsen, P. T. & Johnson, M. A miniature biomimetic sonar and movement tag to study the biotic environment and predator-prey interactions in aquatic animals. *Deep Sea Res. Part I* **148**, 1–11 (2019).
38. Goulet, P. et al. Flash and grab: deep-diving southern elephant seals trigger anti-predator flashes in bioluminescent prey. *J. Exp. Biol.* **223**, jeb222810 (2020).
39. Green, D. B. et al. Modelled mid-trophic pelagic prey fields improve understanding of marine predator foraging behaviour. *Ecography* **43**, 1014–1026 (2020).

40. Kohonen, T. The self-organizing map. *Proc. IEEE* **78**, 1464–1480 (1990).
41. Xi, H., Hieronymi, M., Röttgers, R., Krasemann, H. & Qiu, Z. Hyperspectral differentiation of phytoplankton taxonomic groups: A comparison between using remote sensing reflectance and absorption spectra. *Remote Sens.* **7**, 14781–14805 (2015).
42. Soppa, M. A., Peeken, I. & Bracher, A. Global chlorophyll a concentrations for diatoms, haptophytes and prokaryotes obtained with the diagnostic pigment analysis of HPLC data compiled from several databases and individual cruises https://doi.org/10.1594/PANGAEA.875879 (PANGAEA, 2017). In supplement to: Losa, Svetlana N; Soppa, Mariana A; Dinter, Tilman; Wolanin, Aleksandra; Brewin, Robert J W; Bricaud, Annick; Oelker, Julia; Peeken, Ilka; Gentili, Bernard; Rozanov, Vladimir V; Bracher, Astrid (2017): Synergistic Exploitation of Hyper- and Multi-Spectral Precursor Sentinel Measurements to Determine Phytoplankton Functional Types (SynSenPFT). Frontiers in Marine Science, 4(203), 22 pp, https://doi.org/10.3389/fmars.2017.00203.
43. Vidussi, F., Claustre, H., Manca, B. B., Luchetta, A. & Marty, J.-C. Phytoplankton pigment distribution in relation to upper thermocline circulation in the eastern Mediterranean Sea during winter. *J. Geophys. Res.* **106**, 19939–19956 (2001).
44. Tulet, P. et al. Map-io, an atmospheric and marine observatory program onboard *Marion Dufresne* over the southern ocean. *Earth Syst. Sci. Data Discuss.* **2024**, 1–43 (2024).
45. Thyssen, M. et al. Map-io (Marion Dusfresne Atmospheric Program—Indian Ocean) flow cytometry https://doi.org/10.17882/89505 (2024).
46. Gallon, S. et al. Identifying foraging events in deep diving southern elephant seals, Mirounga leonina, using acceleration data loggers. *Deep Sea Res. Part II* **88-89**, 14–22 (2013). Fourth International Symposium on Bio-logging Science.
47. Viviant, M., Trites, A. W., Rosen, D. A. S., Monestiez, P. & Guinet, C. Prey capture attempts can be detected in steller sea lions and other marine predators using accelerometers. *Polar Biol.* **33**, 713–719 (2010).
48. Sari El Dine, Z. Phytoplankton_ses data. https://doi.org/10.5281/zenodo.11120351 (2024).
49. El Hourany, R. et al. Linking satellites to genes with machine learning to estimate phytoplankton community structure from space. https://doi.org/10.5281/zenodo.10361485 (2024).

Acknowledgements

The elephant seal data were gathered as part of the French National Observatory Mammals as a sampler of the Ocean Environment (SNO-MEMO). Fieldwork in Kerguelen was supported by the French Polar Institute (Institut Polaire Français Paul Emile Victor as part of the IPEV programs 1201 and 1297). This research was financially supported by CNES-TOSCA SOS-Bio Project, by the CNRS funded SNO-MEMO and "Observatoire à Long terme du Vivant", and by the ANR-SOTROC project identified by ANR-24-CE02-3557. We also wish to thank Mark Peter Johnson and Pauline Goulet, who developed the micro-sonar. All animals in this study were treated in accordance with the IPEV ethical and Polar Environment Committee guidelines. ZSED's PhD is funded by CNES and Région Nouvelle Aquitaine. REH acknowledges the ANR Chaire Professeur Junior grant number ANR-22-CPJ1-0003-01, and the graduate school IFSEA that benefits from grant number ANR-21-EXES-0011. We wish to thank Mathilde Chevallay for providing the data on the acoustic size of the prey targeted by SES. MAP-IO was funded by the European Union through the ERDF program, the University of La Réunion, the SGAR-Réunion, the Région Réunion, the CNRS, IFREMER, and the Flotte Océanographique Française. Part of this work was performed with the technical support of the National Center for Remote Sensing, CNRS-Lebanon.

Author contributions

C.G., L.D., and R.E.H. designed research, Z.S.E.D. performed research, Z.S.E.D., M.T., R.E.H., and B.P. contributed new reagents or analytic tools, Z.S.E.D., R.E.H., and B.P. analyzed data, Z.S.E.D., C.G., B.P., M.T., L.D., and R.E.H. wrote the paper. All authors reviewed the paper.

Competing interests

The authors declare no competing interests.

Additional information

Supplementary information The online version contains supplementary material available at https://doi.org/10.1038/s42003-025-08049-0.

Correspondence and requests for materials should be addressed to Ziad Sari El Dine.

Peer review information *Communications Biology* thanks Trevor McIntyre and the other, anonymous, reviewer(s) for their contribution to the peer review of this work. Primary Handling Editors: Eoin O'Gorman and David Favero. A peer review file is available.